A novel image fusion method using WBCT and PCA

Qiguang Miao (苗启广)[1,2] and Baoshu Wang (王宝树)[1]

[1]*School of Computer Science, Xidian University, Xi'an 710071*

[2]*Information & Communication College, Guilin University of Electronic Technology, Guilin 541004*

Received May 29, 2007

A novel image fusion algorithm based on wavelet-based contourlet transform (WBCT) and principal component analysis (PCA) is proposed. The PCA method is adopted for the low-frequency components. Using the proposed algorithm to choose the greater of the active measures, the region consistency test is performed for the high-frequency components. Experiments show that the proposed method works better in preserving the edge and texture information than wavelet transform method and Laplacian pyramid (LP) method do in image fusion. Four indicators for the fusion image are given to compare the proposed method with other methods.

OCIS codes: 100.7410, 100.0100, 100.2000.

Image fusion can process the images obtained from different sensors by a specific algorithm so that the resultant image is more reliable, clearer and more intelligible[1,2]. In recent years, multi-scale and multi-resolution fusion methods are widely used in image fusion field and many research achievements are gotten, for example, wavelet transform method, Laplacian pyramid (LP) method[3].

In capturing the geometry of image edges, however, there are limitations of the commonly used separable extensions of wavelet transforms. Two-dimensional (2D) wavelets are good at isolating the discontinuities at edge points, but do not "see" the smoothness along the contours. Therefore, several transforms have been proposed for image signals, which have incorporated directionality and multiresolution and hence, could capture edges in natural images more efficiently. Steerable pyramid[4], curvelet[5] and contourlets[6] are some popular examples. The contourlet transform is one of the new geometrical image transforms, which can efficiently represent images containing contours and textures[6,7]. Unfortunately, the contourlet transform is a redundancy transform because LP is employed in the first stage. Eslami and Radha proposed a new non-redundant image transform, the wavelet-based contourlet transform (WBCT)[8,9]. WBCT is more appropriate for the analysis of the signals which have line or hyper-plane singularity than wavelet, and it has better approximation precision and sparsity description. When introducing WBCT to image fusion, we can take the features of original images well and provide more information for fusion. The fused image could represent almost the same detail as the original image because WBCT represents edges better than wavelets. Principal component analysis (PCA)[10] is a common tool for image enhancement and data compression. In this paper, we propose a new image fusion method combing WBCT and PCA.

The block structure for WBCT filter bank is shown in Fig. 1 and an example of its frequency partition is shown in Fig. 2. In WBCT, the wavelet transform (WT) captures the point discontinuities, and a direction filter band (DFB) links point discontinuities into linear structures. WBCT involves basis functions that are oriented at 2^N $(N = 1, 2, 3, \cdots)$ directions with flexible aspect ratios. From Fig. 2 we can see that the frequency is divided, where the number of directions is increased with frequency. With such richness in the choice of basis functions, WBCT can represent any one-dimensional (1D) smooth edges with nearly optimal efficiency.

Figure 3 is the decomposition structure of WBCT with 3-scale wavelet decomposition. The direction numbers of DFB are 8, 4, 4. The decomposed image of Barbara is shown in Fig. 4.

The fusion framework using WBCT is shown in Fig. 5. First, the source images are decomposed using WBCT. Suppose that the original images are A and B, the

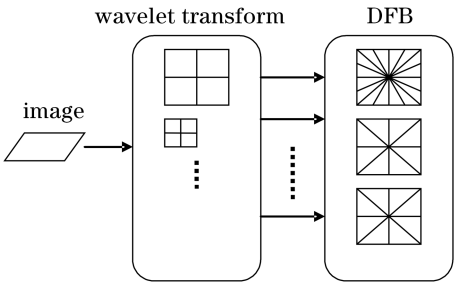

Fig. 1. Framework of WBCT.

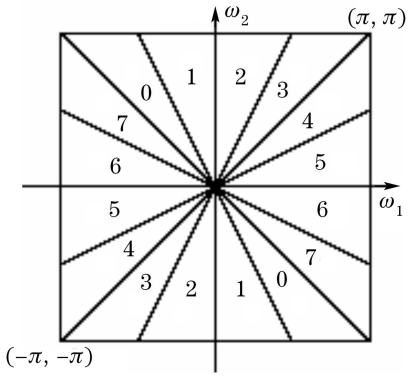

Fig. 2. Frequency partition.

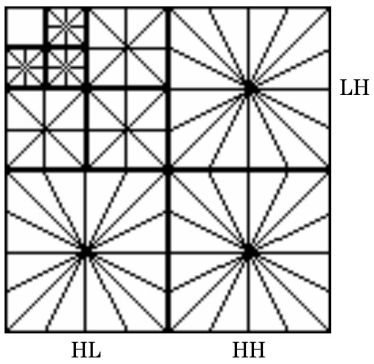

Fig. 3. Decomposition structure of WBCT. L and H represent the low and high frequencies, respectively.

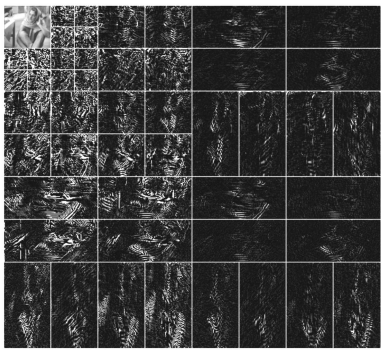

Fig. 4. Subband images of WBCT.

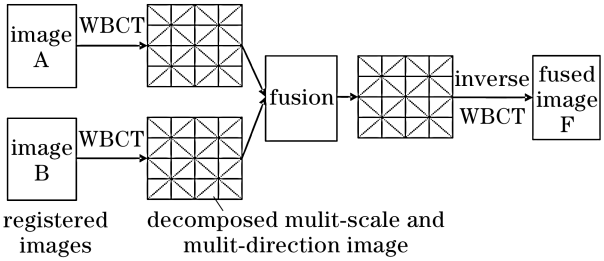

Fig. 5. Fusion framework using WBCT.

corresponding fused image is F. Then the low-frequency and high-frequency components are processed individually.

For the coefficients of the low-frequency components, the PCA method[10] is adopted. The fusion rule of PCA is to get the eigenvalue and the eigenvector of the approximate image, corresponding to the low-frequency components of WBCT. The weights of original images could be gotten based on the eigenvalue, which is very important for multi-modality images. Supposing that $(x, y)^{\mathrm{T}}$ is the eigenvector of the approximate images A and B, the weights of images A and B are

$$W_{\mathrm{A}} = x/(x+y), \quad W_{\mathrm{B}} = y/(x+y). \tag{1}$$

And the fusion coefficient is

$$C_{\mathrm{F}}^{\mathrm{L}}(i,j) = W_{\mathrm{A}} \cdot C_{\mathrm{A}}^{\mathrm{L}}(i,j) + W_{\mathrm{B}} \cdot C_{\mathrm{B}}^{\mathrm{L}}(i,j), \tag{2}$$

where $C_k^{\mathrm{L}}(i,j)$ $(k = \mathrm{A}, \mathrm{B}, \mathrm{F})$ is the coefficient of the low-frequency components for each point.

For the coefficients of the high-frequency components, we firstly calculate the activity measure D_X $(X = \mathrm{A}, \mathrm{B})$ by using decomposition coefficients in neighborhood region. Here, the region energy is chosen because that the more distinctive detail of the feature is, the greater the region energy will be. The region energy of each coefficient of every subband could be gotten by

$$D_X(i,j) = \sum_{i \le M, j \le N} \left(Y_X(i,j)\right)^2, \quad X = \mathrm{A}, \mathrm{B}. \tag{3}$$

By the rule of choosing the greater of the activity measures, we can construct the high-frequency subband coefficients $C_{\mathrm{F}}^{\mathrm{H}}$ of the fused image with

$$C_{\mathrm{F}}^{\mathrm{H}}(i,j) = \begin{cases} C_{\mathrm{A}}^{\mathrm{H}}(i,j), & D_{\mathrm{A}}(i,j) \ge D_{\mathrm{B}}(i,j) \\ C_{\mathrm{B}}^{\mathrm{H}}(i,j), & D_{\mathrm{A}}(i,j) < D_{\mathrm{B}}(i,j) \end{cases}, \tag{4}$$

where $C_{\mathrm{A}}^{\mathrm{H}}(i,j)$ and $C_{\mathrm{B}}^{\mathrm{H}}(i,j)$ are the high-frequency coefficients of A and B, respectively.

And at the same time, the fusion-decision map is also gotten by

$$\mathrm{Map}(i,j) = \begin{cases} 1, & D_{\mathrm{A}}(i,j) \ge D_{\mathrm{B}}(i,j) \\ 0, & D_{\mathrm{A}}(i,j) < D_{\mathrm{B}}(i,j) \end{cases}. \tag{5}$$

The region consistency test is done based on the fusion-decision map. If a certain pixel is to come from source image A but with the majority of its surrounding neighbors from B, this pixel will be switched to come from B. Commonly, the distinctive region is concentrated, so the morphological hole-filling is performed on the fusion-decision map to further improve the decision.

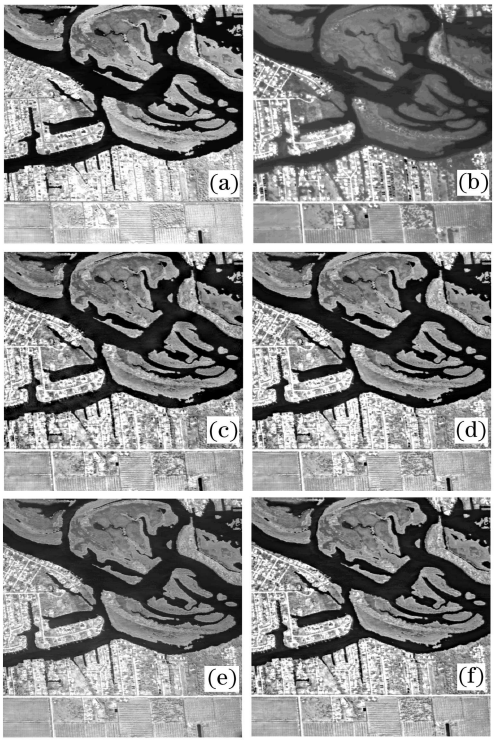

Fig. 6. Fusion of remote images. (a),(b) Band 8 and band 3 remote images; (c)—(f) fusion results with the new method, LP method, controulet method, and SIWT method, respectively.

We tested the proposed WBCT-based fusion scheme as well as the original wavelet-based, LP-based and contourlet-based methods on several images, such as different bands of remote images, hyper-spectral images, and infrared and visual images. The infrared and visual images have a size of 360×270 pixels, and the other images have a size of 512×512 pixels. The WBCT uses 3 wavelet levels and 16 directions at the finest scale. We used 3-level decomposition for shift-invariable wavelet and 6-level decomposition for LP method. The fusion rules of other methods are the same as the WBCT-based method.

Figures 6(a) and (b) are two remote images with different bands. Figure 6(c) shows that the fused image is a clear image with rich features, such as smooth contours and geometric structures. Figures 6(d)—(f) are fused images with LP method, contourlet method and shift-invariable wavelet transform (SIWT) method, respectively. These fused images are better than any one of the source images and all contain much obvious characteristic information of the different band remote images.

Table 1 presents a comparison of the experimental results of image fusion using the four different methods in terms of sharpness, entropy, mean cross entropy (MCE), and root cross entropy (RCE)[11,12]. For the fused image, we hope that the image is clear. The indicator of sharpness shows the clarity of the fused image. And the greater the entropy, the more information is gotten from the original images. MCE and RCE are two indicators which show the differences between the fused images and the original images. The less the MCE and RCE are, the less the differences are. From the indicators given in Table 1, we can see that the sharpness and the entropy are the greatest with the new method. The MCE and RCE of the proposed method are the smallest in the four methods. In a word, the fusion result with the proposed algorithm is the best.

Table 1. Comparison of the Experimental Results of Fig. 6

	Sharpness	Entropy	MCE	RCE
New Method	21.9879	7.5639	3.0013	3.1081
Contourlet Method	21.2295	7.3686	3.1153	3.3232
LP Method	18.0201	7.1856	3.4529	3.4597
SIWT Method	20.8513	7.3125	3.1043	3.2657

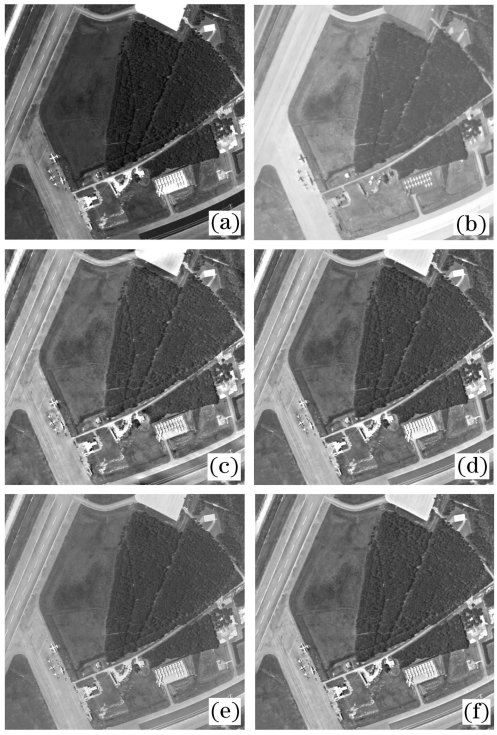

Fig. 7. Fusion of hyper-spectral images. (a),(b) Hyper-spectral images; (c)—(f) fusion results with the new method, LP method, contourlet method, and SIWT method, respectively.

Figures 7(a) and (b) are hyper-spectral images captured by hyper-spectral camera. In Fig. 7(a), the plane, the road and the runway are clear and obvious. In Fig. 7(b), the runway, the road and the plane cannot be seen clearly, but the trees, the grass and the buildings are clear. Figures 7(c)—(f) are fused images by the four different methods, respectively. From the fused images we can see that the fusion results are all satisfying, and the plane, the road, the grass, the sketch of trees, and the buildings are all clear.

From the indicators given in Table 2, we can see that

Table 2. Comparison of the Experimental Results of Fig. 7

	Sharpness	Entropy	MCE	RCE
New Method	14.3796	7.4231	1.1062	1.1616
Contourlet Method	11.9885	7.2535	1.4429	1.4572
LP Method	10.0341	7.1143	1.4306	1.4687
SIWT Method	11.7657	7.2569	1.3930	1.4177

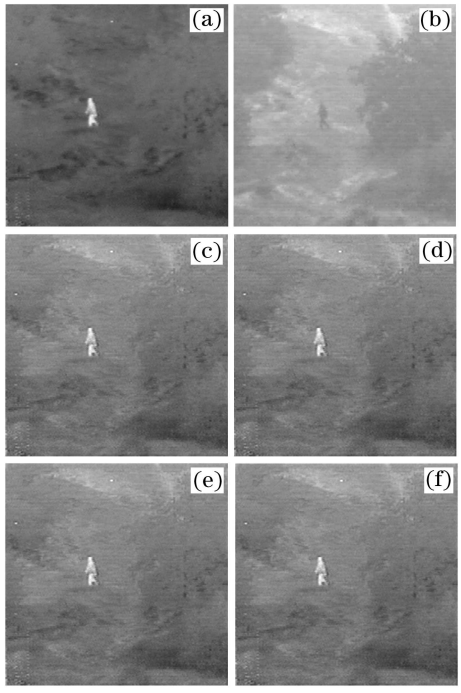

Fig. 8. Fusion of infrared and visual images. (a) Infrared image; (b) visual image; (c)—(f) fusion results with LP method, wavelet method, contourlet method, and the new WBCT method, respectively.

Table 3. Comparison of the Experimental Results of Fig. 8

	Average Gradient	Entropy	MCE	RCE
LP Method	3.7347	1.7936	0.9944	0.9949
Contourlet Method	3.7755	1.7942	0.9905	0.9910
SIWT Method	3.7553	1.7938	0.9796	0.9797
New Method	3.8951	1.8246	0.9664	0.9712

the sharpness and the entropy using the new method are the greatest in the four methods. The MCE and RCE of the proposed method are the smallest in the four different methods. Therefore, the proposed method gives the best fusion results in the four fused images.

Another fusion experiment is done with infrared and visual images, as shown in Fig. 8. Figure 8(a) is an infrared image and Fig. 8(b) is a visual image. In the infrared image, the man is clear and the environment, such as the trees, the hill, the roads, cannot be distinguished. But in the visual image, it is the opposite case. Figures 8(c)—(f) are the fused images using LP method, wavelet transform, contourlet transform, and WBCT method, respectively. From the fusion images, we can see that each method can get satisfactory effect. The man and the environment are all clear.

Table 3 shows the experimental results with the four different methods in terms of average gradient, entropy, MCE, and RCE. From the indicators given in Table 3, we can see that the average gradient and the entropy are the greatest with the proposed method. The MCE and RCE of the new method are the smallest in the four methods. Other image fusion by this algorithm, such as multi-focus images, also proves satisfying, which is in consistency with the experimental results above.

In conclusion, a newly developed method based on WBCT and PCA for image fusion is proposed in this paper. Experimental results by applying the proposed method and other image fusion methods show the effectiveness of the new method.

This work was supported by the National Natural Science Foundation of China (No. 60702063) and the Youth Science Foundation of Guangxi Province (No. 0640067). Q. Miao's e-mail address is qgmiao@mail.xidian.edu.cn.

References

1. Q. Miao, *Research on multi-sensor image fusion methods* (in Chinese) PhD Thesis (Xidian University, 2005).
2. Q. Zhang and B. Guo, Acta Opt. Sin. (in Chinese) **27,** 243 (2007).
3. Q. Miao and B. Wang, Acta Opt. Sin. (in Chinese) **27,** 1605 (2007).
4. E. P. Simoncelli and W. T. Freeman, in *Proceedings of 2nd IEEE International Conference on Image Processing* **3,** 444 (1995).
5. E. J. Candès and D. L. Donoho, in *Proceedings of the in Curve and Surface Fitting 1999* 105 (2000).
6. M. N. Do and M. Vetterli, in *Proceedings of Beyond Wavelets 2002* 1 (2002).
7. M. N. Do, *Directional multiresolution image representations* PhD Thesis (EPFL, 2001).
8. R. Eslami and H. Radha, in *Proceedings of Conference on Information Science and Systems 2004* 784 (2004).
9. R. Eslami and H. Radha, in *Proceedings of Conference on Information Sciences and Systems 2005* http://www.egr.msu.edu/waves/people/Radha_files/2005/ciss05_contourlet.pdf.
10. O. Rockinger, Image Fusion Toolbox[EB/OL], http://www.metapix.de.
11. Q. Miao and B. Wang, Acta Opt. Sin. (in Chinese) **25,** 755 (2005).
12. Y. Wu, W. Yang, and M. Li, Acta Opt. Sin. (in Chinese) **23,** 671 (2003).